J|A|C|S
ARTICLES
Published on Web 07/27/2004

Probing the Structure and Dynamics of End-Grafted Flexible Polymer Chain Layers by Combined Atomic Force−Electrochemical Microscopy. Cyclic Voltammetry within Nanometer-Thick Macromolecular Poly(ethylene glycol) Layers

Jeremy Abbou, Agnès Anne, and Christophe Demaille*

Contribution from the Laboratoire d'Electrochimie Moléculaire, Unité Mixte de Recherche Université−CNRS No. 7591, Université de Paris 7−Denis Diderot, 2 place Jussieu, 75251 Paris Cedex 05, France

Received February 5, 2004; E-mail: demaille@paris7.jussieu.fr

Abstract: The combined atomic force−electrochemical microscopy (AFM-SECM) technique was used in aqueous solution to determine both the static and dynamical properties of nanometer-thick monolayers of poly(ethylene glycol) (PEG) chains end-grafted to a gold substrate surface. Approach of a microelectrode tip from a redox end-labeled PEG layer triggered a tip-to-substrate cycling motion of the chains' free ends as a result of the redox heads' oxidation at the tip and re-reduction at the substrate surface. As few as ∼200 chains at a time could be addressed in such a way. Quantitative analysis of the data, in the light of a simple model of elastic bounded diffusion SECM positive feedback, gave access to the end-tethered polymer layer thickness and the end-to-end diffusion coefficient of the chains. The thickness of the grafted PEG layer was shown to increase with the chain surface coverage, while the end-to-end diffusion coefficient was found to be constant and close to the one predicted by Rouse dynamics. At close tip−substrate separation, slowing of the chains' motion, as a consequence of their vertical confinement within the tip−substrate gap, was observed and quantitatively modeled.

Introduction

The structure of molecular layers formed by attaching linear polymeric chains to surfaces by one of their extremities displays the unique property of being controlled by the chain surface coverage.[1,2] In a good solvent, at coverage low enough for the chains not to overlap, the chains can be statistically viewed as hemispherical blobs (referred to as "mushrooms") of a dimension similar to the free chain Flory radius in solution, R_f.[3] At higher coverage the chains tend to avoid one another by stretching away from the anchoring surface, thus forming a so-called polymer brush. Numerous experimental works[4] have been devoted to the study of the static structure of such polymeric molecular layers. They have largely confirmed the early theoretical predictions in terms of coverage and molecular weight dependence of the layer height or of the monomer distribution within the layer. However, the dynamical properties of end-tethered polymer layers, even though also theoretically explored,[5,6] have proved much more difficult to access experimentally.[7]

We show here that atomic force−electrochemical microscopy (AFM-SECM),[8,9] an electrochemical near-field technique combining atomic force and electrochemical microscopy, can be

(1) (a) Alexander, S. *J. Phys.* **1977**, *38*, 983−987. (b) de Gennes, P. G. *Macromolecules* **1980**, *13*, 1069−1075. (c) Halperin, A.; Tirell, M.; Lodge, T. P. *Adv. Polym. Sci.* **1991**, *100*, 31−71.
(2) (a) Cosgrove, T.; Heath, T.; van Lent, B.; Leermakers, F.; Scheutjens, J. *Macromolecules* **1987**, *20*, 1692−1696. (b) Milner, S. T.; Witten, T. A.; Cates, M. E. *Europhys. Lett.* **1988**, *5*, 413−148. (c) Milner, S. T.; Witten, T. A.; Cates, M. E. *Macromolecules* **1988**, *21*, 2610−2619. (d) Milner, S. T. *Science* **1991**, *251*, 905−914. (e) Lai, P.-Y.; Zhulina, E. B. *J. Phys. II* **1992**, *2*, 547−560. (f) Grest, G.; Murat, M. M*acromolecules* **1993**, *26*, 3108−3117. (g) Binder, K. *Eur. Phys. J. E* **2002**, *9*, 293−298.
(3) Flory, P. *Principles of Polymer Chemistry*; Cornell University Press: Ithaca, NY, 1971.
(4) (a) Auroy, P.; Auvray, L.; Léger, L. *Phys. Rev. Lett.* **1991**, *66*, 719−722. (b) Field, J. B.; Topakcioglu, C.; Dai, L.; Hadziioannou, G.; Smith, G.; Hamilton, W. *J. Phys. II* **1992**, *2*, 2221−2235. (c) Field, J. B.; Topakcioglu, C.; Ball, R. C.; Stanley, H. B.; Dai, L.; Barford, W.; Penfold, J.; Smith, G.; Hamilton, W. *Macromolecules* **1992**, *25*, 434−439 (d) Auroy, P.; Mir, Y.; Auvray, L. *Phys. Rev. Lett.* **1992**, *69*, 93−95. (e) Marzolin, C.; Auroy, P.; Deruelle, M.; Folkers, J. P.; Léger, L.; Menelle, A. *Macromolecules* **2001**, *34*, 8694−8700.
(5) (a) Halperin, A.; Alexander, S. *Europhys. Lett.* **1988**, *6*, 329−334. (b) Klushin, L. I.; Skvortsov, A. M. *Macromolecules* **1991**, *24*, 1549−1553.
(6) (a) Murat, M.; Grest, G. S. *Macromolecules* **1989**, *22*, 4054−40597. (b) Binder, K.; Lai, P.-Y. *J. Chem. Phys.* **1991**, *95*, 9288−9299. (c) Binder, K.; Lai, P.-Y.; Wittmer, J. *Faraday. Discuss.* **1994**, *98*, 97−109. (d) Neelov, I. M.; Binder, K. *Macromol. Theory Simul.* **1995**, *4*, 1063−1084.
(7) (a) Fytas, G.; Anastasiadis, S. H.; Seghruochni, R.; Vlassopoulos, D.; Li, J.; Factor, B. J.; Theobald, W.; Toprakcioglu, C. *Science* **1996**, *274*, 2041−2044. (b) Monkenbush, M.; Schneiders, D.; Richter, D.; Farago, B.; Fetters, L.; Huang, J. *Physica B* **1995**, *213*, 707−711. (c) Zeghal, M.; Deloche, B.; Auroy, P. *Macromolecules* **1999**, *32*, 4947−4955. (d) Kremer, F.; Hartmann, L.; Sergei, A.; Pouret, P.; Léger, L. *Eur. Phys. J. E* **2003**, *12*, 139−142.
(8) (a) *Scanning Electrochemical Microscopy*; Bard, A. J., Mirkin, M. V., Eds.; Marcel Dekker: New York, 2001. (b) Bard, A. J.; Fan, F.-R. F.; Mirkin, M. V. In *Electroanalytical Chemistry*; Bard A. J., Ed.; Marcel Dekker: New York, 1994; Vol. 18, p 243.
(9) (a) Macpherson, J. V.; Unwin, P. R. *Anal. Chem.* **2000**, *72*, 276−285. (b) Macpherson, J. V.; Webb, M. A.; Unwin, P. R. *Anal. Chem.* **2001**, *73*, 550−557. (c) Kranz, C.; Friedbacher, G.; Mizaikoff, B.; Lugstein, A.; Smoliner, J.; Bertagnolli, E. *Anal. Chem.* **2001**, *73*, 2491−2500. (d) Kranz, C.; Kueng, A.; Mizaikoff, B.; Lugstein, A.; Bertagnolli, E. *Angew. Chem., Int. Ed.* **2003**, *42*, 3238−3240.

used to determine both the static and dynamical properties of end-tethered molecular layers of redox-tagged poly(ethylene glycol) (PEG) chains in aqueous solution, a good solvent for such chains.

Custom-synthesized heterobifunctional linear Fc-PEG_{3400}-NHS molecules, made of poly(ethylene glycol) chains of molecular weight 3400, bearing at one end a ferrocene (Fc) head and at the other an *N*-hydroxysuccinimide activated ester (NHS), are covalently attached to an amine-bearing gold substrate surface, thus yielding a well-defined polymeric layer of controllable chain coverage. When a nanometer-sized spherical microelectrode, mounted as a combined AFM-SECM probe and biased at a positive enough potential, is approached from the gold substrate, the ferrocene heads borne by the substrate-anchored PEG chains can be oxidized into ferricenium (Fc^+) at the microelectrode and subsequently reduced back to their ferrocene state by the appropriately biased substrate. The ensuing tip-to-substrate cycling of the ferrocene heads is controlled only by the chain flexibility; therefore, the recorded tip current directly reflects the dynamics of the chain movement that can thus be characterized quantitatively. The microelectrode tip can be precisely positioned within the few-nanometers-thick polymer layer and the steady-state cyclic voltammogram of the ferrocene heads recorded, thus giving access to the parameters of the microelectrode reaction.

The small size of the spherical microelectrode and the amplifying effect of the tip-to-substrate cycling of the ferrocene heads allow us to address a very limited number of chains, thus probing the dynamics of a few hundred chains at a time. Moreover, the force-sensing capabilities of the combined AFM-SECM probe allow us to measure the dynamical response of the chains while continually compressing the polymer layer. The thus-measured static (height) and dynamical (diffusion coefficient) properties of the molecular layer are then studied as functions of the chain coverage.

Direct electrochemical measurements at a microelectrode penetrating a 0.2-μm-thick redox-polymer *film* have been previously reported in the pioneering work of Bard and coworkers.[10] In contrast, here it is a *single molecular layer* of end-grafted nanometer-sized macromolecules that is probed by the AFM-SECM combined technique.

Experimental Section

PEG_{3400} Derivatives and Materials. Poly(ethylene glycol) (PEG) 3400 monoacid, *O*-(2-carboxyethyl)poly(ethylene glycol) 3400 (OH-PEG_{3400}-CO_2H), and *O*-2-[*N*-hydroxysuccinimidylethyloxycarbonyl]-*O*′-2-(*N*-biotinamidoethyl)poly(ethylene glycol) 3400 (Biotin-PEG_{3400}-NHS, average molecular weight 3500, average number of OCH_2CH_2 monomer units $N = 77$) were from Nektar Therapeutics, Huntsville, AL (formerly Shearwater Polymers). The Fc-PEG_{3400}-OH conjugate was prepared from poly(ethylene glycol) 3400 monoacid (OH-PEG_{3400}-CO_2H) as previously described.[11] Prior to NHS activation, the Fc-PEG_{3400}-OH sample was purified onto a Waters C18 μBondapak 125-Å, 10-μm HPLC column and evaluated for its molecular mass distribution by matrix-assisted laser desorption/ionization time-of-flight (MALDI-TOF) mass spectrometry. MALDI-TOF MS for Fc-PEG_{3400}-OH, (+) data: m/z $(M + Na)^+$; the distribution of peaks (repeating units = 44 u) corresponded to average $N = 79$, $C_{173}H_{335}FeNNaO_{81}$ requires 3804.35; polydispersity index P 1.01. Fc-PEG_{3400}-NHS was prepared from Fc-PEG_{3400}-OH using the activating coupling reagent *N*,*N*-disuccinimidyl carbonate (DSC) as previously reported. In the present study, the resulting activated NHS ester was precipitated from the reaction mixture by addition of diethyl ether, washed copiously with ether, and then redissolved in dichloromethane. The solution was passed onto a 0.22-μm Millipore Miltex membrane and evaporated to yield Fc-PEG_{3400}-NHS, which was finally dried and stored in vacuo at 4 °C. All experiments were performed at ambient temperature unless otherwise specified.

2-Aminoethanethiol (cysteamine, >98%) and sodium perchlorate ($NaClO_4$) monohydrate were purchased from Fluka and Merck, respectively. Other commercial chemicals were reagent grade or better quality and used as received. All aqueous solutions were made with Milli-Q purified water (Millipore). Phosphate buffer (0.1 M ionic strength) was made of 49 mM KH_2PO_4, pH-adjusted to 7.0 with a 1 M NaOH solution. All solvents used for PEG grafting of gold substrate surfaces as well as AFM-SECM experiments were filtered before use on a 0.22-μm nylon Cameo filter.

Preparation of the Template-Stripped Gold Substrate Surface. The smooth gold-on-mica substrates were prepared following a procedure reported in the literature.[12] Briefly, a mica sheet was cleaved just before being put into the vacuum chamber of a BOC Edwards auto 306 vacuum system, 20 cm above pure gold (99.999%), which was then evaporated under a pressure of 2×10^{-6} mbar onto the mica surface at the rate of 0.1 nm/s (the deposition rate was controlled by a quartz balance). The evaporation was considered to be complete after a 200-nm-thick layer had been deposited. The gold-covered mica sheet was then glued (epotek 377) onto a glass slide, which had previously been rinsed with both Milli-Q water and acetone, and baked in an oven at 150 °C for 1.5 h. The mica−gold−glass sandwich thus obtained could be stored for several months without the gold surface being altered. The gold surface was separated from the mica just before use. This was accomplished by soaking the sandwich in THF for 2 min and then pulling the mica from the flat gold surface-bearing glass slide. The gold surface was then rinsed successively with ethanol and Milli-Q water. Tapping-mode AFM characterization of the freshly stripped surface was carried out using conventional AFM probes (~10 nm radius). The surface topography consisted of ~200-nm-wide, extremely flat plateaus separated by narrow valleys (~20 nm in width). Only the surfaces having an average roughness of <1 nm were immediately thiolated with cysteamine. When required, evaluation of the effective area of the gold substrates was carried out as previously reported,[13] by integration of the reduction peak of the gold oxide monolayer formed by cycling the substrate in a 0.5 M H_2SO_4 solution between +0.3 and +1.6 V/SCE at 0.2 V/s and resting for 5 min at a potential of ca. +1.5 V/SCE.[14] We reproducibly found an effective substrate surface area of 2.5 cm^2 (corresponding to a roughness of ~2) and thus used this value to calculate the chain surface coverage as described in the text. In a separate experiment, we imaged the substrate in tapping-mode AFM during electrochemical cycling in order to make sure that this process did not disrupt the template-stripped gold surface.

Preparation of the End-Grafted PEG Monolayers on Gold Substrate Surface. The liquid cell in which the gold substrate surface was mounted was filled with a 5 mM cysteamine solution in ethanol (filtered through a 0.05-μm Isopore Millipore membrane) and kept for 2 h under a nitrogen atmosphere, after which the surface was thoroughly rinsed with ethanol and Milli-Q water. A Fc-PEG_{3400}-NHS solution in phosphate buffer, pH 7, was then introduced into the liquid cell and

(10) Mirkin, M. V.; Fan, F.-R. F.; Bard, A. J. *Science* **1992**, *257*, 364−366.
(11) Anne, A.; Moiroux, J. *Macromolecules* **1999**, *32*, 5829−5835.
(12) (a) Hegner, M.; Wagner, P.; Semenza, G. *Surf. Sci.* **1993**, *291*, 39−46. (b) Wagner, P.; Hegner, M.; Güntherodt, H.-J.; Semenza, G. *Langmuir* **1995**, *11*, 3867−3875.
(13) Anne, A.; Demaille, C.; Moiroux, J. *Macromolecules* **2002**, *35*, 5578−5586.
(14) (a) Michri, A. A.; Pshenichnikov, A. G.; Burshtein, R. *Kh. Elecktrokhim.* **1972**, *8*, 364−366. (b) Rand, D. A. J.; Woods, R. *J. Electroanal. Chem.* **1972**, *35*, 209−218. (c) Cadle, S. H.; Bruckenstein, S. *Anal. Chem.* **1974**, *46*, 16−20. (d) Trasatti, S.; Petrii, O. A. *Pure Appl. Chem.* **1991**, *63*, 711−734.

left to react with the cysteamine-derivatized surface. The final chain grafting coverage was adjusted by varying the Fc-PEG_{3400}-NHS solution concentration (from 0.5 to 20 mM) and the reaction time (from 3 to 15 min). As previously observed,[13] any further increase of the reaction time or Fc-PEG_{3400}-NHS concentration did not yield any noticeable increase in the PEG surface concentration. The saturation surface coverage of $\sim 2 \times 10^{-11}$ mol/cm^2 of effective surface area that we obtained was quite close to the values reported in the literature for the covalent attachment of PEG chains to various solid surfaces.[15] However, this value is slightly higher than the one we previously reported, $\sim 0.8 \times 10^{-11}$ mol/cm^2, which could be grafted onto the surface of polished gold disk microelectrodes.[13] This difference might arise from the higher degrees of cleanliness and homogeneity of the evaporated gold surfaces when compared to polished resin-embedded polycrystalline gold wire surfaces. Prior to the AFM-SECM experiment, the surface was thoroughly rinsed with Milli-Q water. When not in use, the Fc-PEG-grafted gold surfaces were stored at room temperature in deaerated Milli-Q water. A typical decrease of ca. 15% in the surface coverage was observed after the first overnight storage of ca. 16 h. Beyond the first overnight storage, the PEG-modified gold surfaces exhibit good stability and can be used for a week with no appreciable changes in the electrochemical response.

Fabrication and Characteristics of the Combined AFM-SECM Probes. The combined AFM-SECM probes bearing submicrometer-sized spherical electrode tips were fabricated as previously reported.[16] Briefly, a ~5-mm-long, 60-μm-diameter gold wire was bent to a right angle ~1 mm away from one of its ends while its other end was flattened between stainless steel plates. The short extremity of the wire was then etched electrochemically and its very end thus given a roughly conical shape. A spark discharge of controlled intensity was then used to locally fuse the very end of the wire, which rounded up instantaneously upon cooling. As previously shown,[16] the arc discharge microelectrode fabrication technique allows a reproducible control of the tip geometry. In the present work, the spark generator was set to generate exclusively spherical tips having a diameter in the 0.4−0.8-μm range. Even though smaller tips can be fabricated using this technique, we chose this tip size range so that the recorded currents in AFM-SECM experiments were in an easily measurable range of ~10 pA. The surface of the spherical tip end was shown by scanning electron microscopy imaging to be extremely smooth (no corrugation could be seen even at a magnification of ×200 000). The probe was then entirely insulated by deposition of electrophoretic paint and was glued onto a standard AFM silicon chip. Shortly before use, a high-voltage pulse was applied to the probe to selectively expose its spherical tip end. To remove any residual contaminant, the tip was finally electrochemically cleaned by immersing its very end in a 0.5 M H_2SO_4 solution while scanning its potential between +0.3 and +1.8 V/SCE at 2 V/s for about 10 cycles. We limited the number of experiments using the same tip to three in order to minimize the risk of destroying the tip during handling. The exact value of the spherical tip radius was determined by scanning electron microscopy as described below and used when required for data interpretation, thus ensuring comparability between the data from separate experiments.

Scanning Electron Microscopy Imaging of the Probes. Images were acquired using a LEO S440 scanning electron microscope (SEM) at an electron beam energy of 20 keV. The probes were imaged as-is; that is, they were not coated with a thin metal sputtered layer. The probes were systematically imaged after they were used in AFM-SECM experiments in order to measure the tip radius, R_{tip}, and the cantilever thickness, t. The images showed that the spherical shape of the tip was not altered by the repeated tip-to substrate contact occurring unavoidably during AFM-based experiments. This was a benefit of the appropriate cantilever flexibility. Within the SEM resolution scale, the lower parts of the tips were seen to be hemispherical. It therefore seemed reasonable to assume that the hemispherical geometry was preserved even at the very bottom section of the tips actually "seen" by the nanometer-sized chains. (See Supporting Information for SEM images of one of the tips used here.)

In order to be imaged, the probes were irreversibly glued onto conductive supports and thus could not be reused after SEM imaging.

Calculation of the Spring Constant of the Combined Probes. The spring constant of the combined probe, k_{probe}, was calculated from the measured dimensions of the flattened part of the wire-based probe, which acted as a rectangular cantilever, using the formula[17a] $k_{probe} = Ewt^3/4l^3$, where w, t, and l stand respectively for the cantilever width, thickness, and length and E is the elastic modulus of gold (~80 Gpa).[18] Even though w and l were carefully measured using an optical microscope and t using a scanning electron microscope, we estimated the resulting accuracy on the value of k_{probe} to be not better than $\sim \pm 50\%$. This poor accuracy is mostly a consequence of the cubic dependence of the spring constant on the cantilever thickness (see the above expression). We are currently trying to adapt reported spring constant calibration techniques[17b] to determine more accurately the spring constant of our made-AFM combined probes. In the work reported here, three different combined probes, labeled p1, p2, and p3, were used. Their tip radii were respectively of 225, 335, and 400 nm, and their spring constants were 0.5, 1, and 5 nN/nm. Probe p1 was used for the experiments presented below, corresponding to a Fc-PEG surface concentration, Γ, of 0.5, 1, and 2×10^{-11} mol/cm^2. Probes p2 and p3 were respectively used for the experiments carried out at $\Gamma = 1.25 \times 10^{-11}$ and 1.75×10^{-11} mol/cm^2.

AFM-SECM Experiments. The AFM/SECM experiments were performed with a Molecular Imaging PICOSPM AFM microscope (Scientec, France) that was equipped with a fluid cell containing an aqueous 1 M $NaClO_4$ electrolyte solution. A homemade bipotentiostat enabled us to independently apply the electrochemical tip and substrate potentials with respect to a quasi-reference electrode (an AgCl-coated silver wire). The counter electrode was a platinum wire. The quasi-reference electrode was calibrated against a KCl saturated calomel electrode (SCE). The tip and substrate currents were measured by the high (100 pA/V) and low (20 μA/V) gain current measuring circuits of the bipotentiostat. The substrate potential was generated by a PAR175 programmer, and the substrate current data were acquired on a digital oscilloscope. The Molecular Imaging PICOSCAN controller was used to generate the tip potential and to acquire the tip current data. The tip biasing circuit was kept opened when the tip was at rest on the surface, that is, when the AFM force feedback loop was *on*. As a result, no long-lasting tip−substrate short-circuit could occur. During AFM-SECM experiments, the tip movement and potential were under the control of a homemade script program that performed the subsequent tasks. The program was in charge of withdrawing the tip from the surface before closing the tip biasing circuit. The tip was then set to its assigned potential and equilibrated for a few seconds before any approach curve or cyclic voltamogram was recorded. After that, the script program opened the tip circuit before restoring the feedback loop, which brought the tip back to its resting position in contact with the surface. Thanks to this fully automated procedure, only occasional brief tip−substrate short-circuits occurred during approach curves but were noticed to have no consequence on the tip performance in subsequent

(15) (a) Burns, N. L.; Van Alstine, J. M.; Harris, J. M. *Langmuir* **1995**, *11*, 2768−2776. (b) Sofia, S. J.; Premnath, V.; Merill, E. W. *Macromolecules* **1998**, *31*, 5059−5070. (c) Lu, H. B.; Campbell, C. T.; Castner, D. G. *Langmuir* **2000**, *16*, 1711−1718. (d) Tokumitsu, S.; Liebich, A.; Herrwerth, S.; Himmelhaus, M.; Grunze, M. *Langmuir* **2002**, *18*, 8862−8870. (e) Sharma, S.; Johnson, R. W.; Desai, T. A *Langmuir* **2004**, *20*, 348−356.
(16) Abbou, J.; Demaille, C.; Druet, M.; Moiroux, J. *Anal. Chem.* **2002**, *74*, 6355−6363.
(17) (a) Sader, J. E.; Chon, J. W. M.; Mulvaney, P. *Rev. Sci. Instrum.* **1999**, *70*, 3967−3969. (b) Burnham, N. A.; Chen, X.; Hodges, C. S.; Matei, G. A.; Thoreson, E. J.; Roberts, C. J.; Davies, M. C.; Tendler, S. J. B. *Nanotechnology* **2003**, *14*, 1−6.
(18) Sader, J. E.; Larson, I.; Mulvaney, P.; White, L. R. *Rev. Sci. Instrum.* **1995**, *66*, 3789−3798.

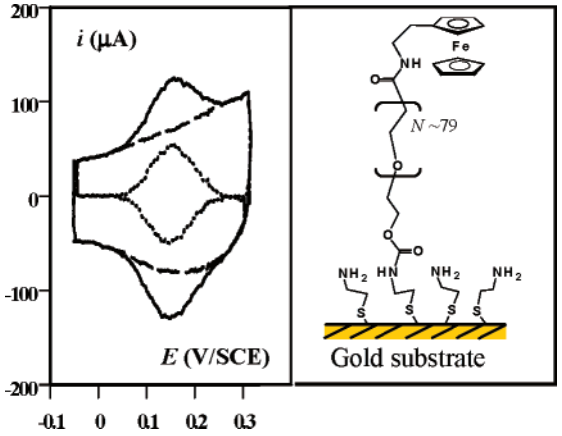

Figure 1. (Left) Cyclic voltammogram at the gold substrate electrode bearing end-grafted Fc-PEG_{3400} chains. Solid line, cyclic voltamogram of the Fc-PEG bearing substrate; dashed line, background signal recorded after the Fc-PEG layer had been electrochemically stripped; dotted line, background-corrected signal. Signals were numerically filtered (see Supporting Information). Grafting surface concentration, $\Gamma = 2 \times 10^{-11}$ mol/cm^2; scan rate, $\upsilon = 2$ V/s; 1 M $NaClO_4$ supporting electrolyte; effective surface, area 2.5 cm^2. (Right) Schematic representation of the grafted redox monolayer.

approaches. The AFM built-in controller interface allowed the tip, once withdrawn from the surface, to be translated over it between approach curves.

The tip movement was monitored via the reflection of the AFM laser onto the cantilever arm of the probe and the detection of the reflected beam on a position-sensitive detector (PSD). The PSD was calibrated in situ using its linear response with the piezo elongation.

For each experiment, dozens of AFM-SECM approach curves were acquired at different locations on the substrate. The deflection approach curves presenting interference peaks due to the laser-based tip-tracking system[17b] were not considered for further analysis. As a result, for each individual experiment, only 5−10 of the simultaneously acquired current and deflection approach curves were fitted using the theoretical expressions reported below. In some cases, after several approach curves had been recorded, we noted a partial loss of the tip current response, probably as a result of tip contamination. The full magnitude of the current signal was restored after the tip had been withdrawn from the surface and cycled in situ between −0.3 and +1.2 V vs Ag/AgCl QRE at 0.5 V/s. During the measurements, the microscope head was placed inside a homemade vibration-proof Faraday cage.

Results

Terminal Attachment of the PEG Chains to the Gold Substrate Surface. The surface of a template-stripped gold substrate was modified by reaction with cysteamine ($HS-CH_2-CH_2-NH_2$) as described in the Experimental Section. The thus-obtained amine-functionalized surface was subsequently reacted with NHS-terminated PEG chains bearing, at the other extremity, either redox-active alkyl-ferrocene (Fc) or electro-inactive Biotin. This resulted in the covalent end-grafting of the chains to the surface via a stable amide-type bond, as sketched in Figure 1.

Cyclic Voltammetry of the Substrate Bearing an End-Grafted Fc-PEG Layer: Measurement of the PEG Surface Coverage. When ferrocene-tagged PEG chains were immobilized, the chain surface coverage could be conveniently measured by recording the cyclic votammogram of the substrate immersed in an aqueous solution containing 1 M $NaClO_4$ as a supporting electrolyte.

At a slow enough scan rate υ, a characteristic reversible Nerstian surface voltammogram[19] was recorded (Figure 1). The separation between the peak potentials of the anodic and cathodic waves was small, <20 mV at 1 V/s, and the peak currents of the waves were proportional to the scan rate, while the current coincided with the background current at potentials much larger or much smaller than the peak potentials (see Figure 1). The surface standard potential of the PEG-chain-borne Fc/Fc^+ redox couple, $E° = 150 \pm 10$ mV/SCE, as evaluated from the average value of the anodic and cathodic peak potentials, was in agreement with earlier reported values.[13,20] Such voltammetric behavior ensures that all the ferrocene heads are given ample time to reach the substrate and to reversibly exchange an electron with it. Therefore, the surface concentration, Γ, of ferrocene heads, and consequently of PEG chains, present at the surface could be determined by integrating the voltammetric signals[19] (see Supporting Information for details). By adjusting the grafting conditions, PEG layers of surface concentration varying from 0.5×10^{-11} mol/cm^2 up to a saturation coverage of 2×10^{-11} mol/cm^2 could be prepared for AFM-SECM characterization (see Experimental Section). Interestingly, the peak potentials of the surface signals were the same whatever the Fc-PEG surface concentration. This shows that the aqueous environment experienced by the ferrocene heads was similar in all cases.

When electroinactive Biotin-PEG_{3400} chains instead of Fc-PEG_{3400} chains were grafted onto the substrate, no Faradaic signal was recorded, as anticipated. Due to the similar size and hydrophobic properties of Fc and Biotin heads, we can reasonably assume in the following that similar amounts of Fc-PEG and Biotin-PEG chains could be end-grafted onto a gold surface when identical PEG chain length and derivatization conditions are considered.[11]

Tip Deflection and Tip Current Approach Curves of the End-Grafted PEG Layers in a 1 M $NaClO_4$ Aqueous Solution. (a) Tip Deflection versus Distance Response. As represented schematically in Figure 2, the combined AFM-SECM probe was pushed by the supporting piezo toward a gold substrate bearing an end-grafted Fc-PEG layer.

Z_{tip}, the tip displacement away from its resting position, was plotted as a function of the imposed piezo elongation, Z_{piezo}. The resulting characteristic AFM deflection approach curve, as shown in Figure 2b, can be divided into three zones (labeled I, II, III). In zone I, the tip is too far away to sense the substrate and is at rest. In zone II, the tip starts to compress the polymer layer, which deforms under load, and the cantilever arm supporting the tip bends upward. In zone III, the tip has made hard contact with the substrate and moves linearly with the piezo. It is noteworthy that no "jump to contact" was recorded on the approach curve, as the short-range forces usually responsible for such a phenomenon were probably screened out by the large repulsive forces resulting from the compression of the polymer layer. When the tip was pulled away from the surface, the retraction curve recorded at that time, once corrected for the piezo hysteresis, could be exactly superimposed on the

(19) Laviron, E. In *Electroanalytical Chemistry*; Bard, A. J., Ed.; Marcel Dekker: New York, 1982; Vol. 12, pp 53−157.
(20) (a) Anne, A.; Demaille, C.; Moiroux, J. *J. Am. Chem. Soc.* **1999**, *121*, 10379−10388. (b) Demaille, C.; Moiroux, J. *J. Phys. Chem. B.* **1999**, *103*, 9903−9909. (c) Anne, A.; Demaille, C.; Moiroux, J. *J. Am. Chem. Soc.* **2001**, *123*, 4817−4825.

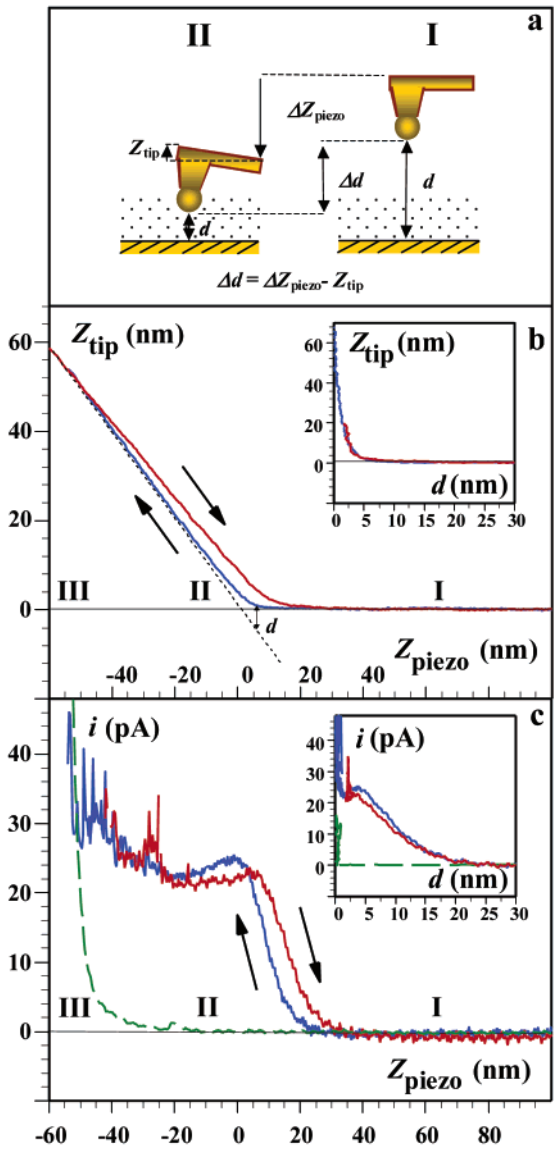

Figure 2. (a) Representative deflection behavior of a combined AFM-SECM probe partially penetrating a substrate-grafted polymer layer (represented as a dotted area). (I) The gold tip is in solution far away from the substrate and thus not deflected. (II) Upon further approach by an increment ΔZ_{piezo}, the tip is brought in contact with the layer and starts to compress it. As a result, the flexible cantilever arm bends upward by an amount Z_{tip}. When in region III, the tip has made hard contact with the substrate. Simultaneously recorded tip deflection (b) and tip current (c) vs piezo elongation Z_{piezo} curves for a gold substrate bearing redox Fc-PEG_{3400} chains (continuous lines) or Biotin-PEG_{3400} chains (dashed line in (c); the retraction curve is not represented). The dotted line in (b) is used to show graphically how the tip-to-substrate distance, *d*, is determined and how the $Z_{piezo} = 0$ point is defined. The insets in (b) and (c) show the respective replots of the curves as a function of *d*, derived as explained in the text. $\Gamma = 2 \times 10^{-11}$ mol/cm^2. Gold substrate potential, E_{sub}, was held at -0.1 V/SCE; the tip bias, $E_{tip} = +0.4$ V/SCE; 1 M $NaClO_4$ supporting electrolyte.

approach curve (see inset in Figure 2b). No negative deflection, indicative of adhesion or chain elongation, was observed on the retraction curve. The cantilevers of the homemade probes used here are probably too stiff to detect such phenomena.

(b) Tip Current versus Distance Response. The bipotentiostat allowed the tip current to be measured, so that a current approach curve plotting the tip current versus Z_{piezo} could be acquired simultaneously with the deflection curve, as presented in Figure 2c. The tip and substrate were respectively biased at potentials largely positive ($E_{tip} = +0.4$ V/SCE) and sufficiently negative ($E_{sub} = -0.1$ V/SCE) with respect to the ferrocene head standard potential ($E° = +0.15$ V/SCE). When the tip was far away from the substrate (zone I of the deflection curve), no current was detected. However, upon further approach (zone II), a current started to flow through the tip and increased while the tip was further pressed against the polymer layer until a broad current peak was reached. Further compression of the Fc-PEG layer resulted in a slight decrease, followed by a sudden jump of the current as zone III was reached. Upon reversal of the piezo movement, a tip current retraction curve was recorded that was very similar to, albeit slightly less intense than, the tip current forward curve. The hysteresis seen is largely due to the nonlinear piezo response. When the same experiment was conducted over a Biotin-PEG layer instead of a Fc-PEG layer, the same tip deflection curve as reproduced in Figure 2b was obtained. However, a drastically different tip current approach curve was detected (see dashed curve in Figure 2c) as no current was detected in zone II, although the tip was touching and indeed compressing the layer. Only the abrupt current rise of zone III, indicative of tunneling, was then recorded.

Monitoring both the tip and piezo movements allowed the critical distance, *d*, separating the tip from the substrate to be derived: $\Delta d = \Delta Z_{piezo} - Z_{tip}$ (see Figure 2a). From this expression and as graphically represented in Figure 2b, it is seen that the "hard-contact" contact point between the tip and the gold substrate surface, i.e., $d = 0$, corresponds to the linear portion (zone III of Figure 2b) of the force curve, which is reached asymptotically in the Z_{piezo} scale. Admittedly, although this way of defining the "hard-contact" point is usually employed in AFM experiments, it is not error-free as, in the linear portion of the force curve, a thin, stiffened layer of polymer may be sandwiched between the tip and substrate.[21] Definition of a $Z_{piezo} = 0$ point, as represented in Figure 2b, is convenient as it allows us to visualize the tip−substrate contact point *had the polymer layer not been present*, but it is in no way required for the above *d* calibration. It should also be kept in mind that this $Z_{tip} = 0$ point does not correspond to the onset of the approaching tip−grafted layer contact. Indeed, no such sharp contact point is expected here as the contact is first made with the outer edge of the end-grafted layer which is by nature a diffuse and compliant surface.[22] In other words, the monomers of end-grafted polymers are predicted to be distributed away from the grafting surface, following a smoothly decaying profile,[2] so that no clear-cut grafted layer/solution boundary can be defined other than statistically.

The deflection and current approach curves shown respectively in parts b and c of Figure 2 were then replotted as a function of *d* in the corresponding insets. Although virtually no tip deviation was recorded at $d > 10$ nm, the current was observed to increase gradually when the tip was 30 nm away from the surface, to reach its maximum at $d \approx 4$ nm, and decreased slowly until tunneling occurred at $d = 0$. The onset of tunneling was noticed to correspond to the $d = 0$ point within an accuracy of ± 1 nm, thus validating the above force curve-based "hard-contact" point determination.

(21) (a) Overney, R. M.; Leta, D. P.; Pictroski, C. F.; Rafailovich, M. H.; Liu, Y.; Quinn, J.; Sokolov, J.; Einsenberg, A.; Overney, G. *Phys. Rev. Lett.* **1996**, *76*, 1272−1275. (b) Braithwaite, G. J. C.; Howe, A.; Luckham, P. F. *Langmuir* **1996**, *12*, 4224−4237.
(22) Israelachvili, J. *Intermolecular and Surface Forces*, 2nd ed.; Academic Press: San Diego, CA, 1992; pp 288−298.

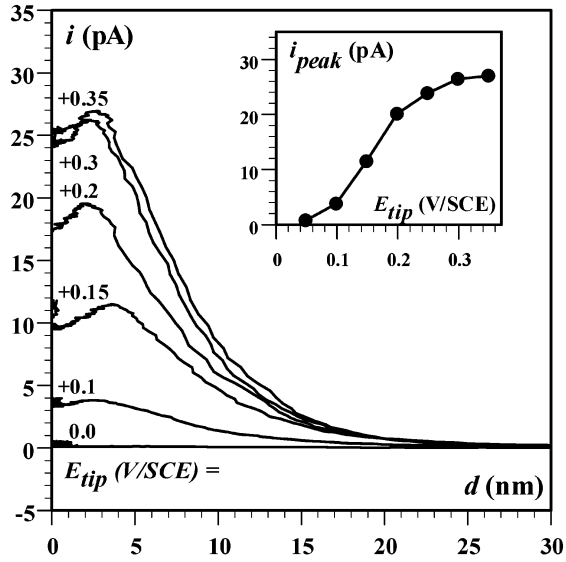

Figure 3. Dependence of the tip current vs distance approach curves on the applied tip potential. The value of the tip potential, E_{tip}, is indicated on the curve. The inset shows the variation of the peak current of the approach curve, i_{peak}, as a function of the tip potential. $E_{sub} = -0.1$ V/SCE; $\Gamma = 2 \times 10^{-11}$ mol/cm^2; 1 M $NaClO_4$ supporting electrolyte.

Both the tip deflection and tip current approach curves were highly reproducible and could be recorded repeatedly either at the same spot on the surface or after the tip had been translated along it (hovering). In some cases, however, typically after tens of approach curves were recorded, an in situ cleaning of the tip was required, which was carried out by cycling the tip potential as detailed in the Experimental Section. Subsequently, the tip current signal was fully recovered. We observed that increasing the $NaClO_4$ supporting electrolyte concentration from 1 to 2 M did not change the approach curves. Varying the tip approach speed from 10 to 50 nm/s had also no effect, which supports the fact that the recorded tip currents were indeed stationary, i.e., time independent.

(c) Tip Potential Dependence of the Tip Current versus Distance Approach Curve. Tip deflection and current approach curves were simultaneously recorded over Fc-PEG derivatized substrates for different values of the tip potential, E_{tip}, ranging from -0.1 to $+0.4$ V/SCE, the substrate potential being held constant at -0.1 V/SCE. Regardless of the tip potential, deflection curves such as the one shown in Figure 2b were recorded. Conversely, the tip current versus distance approach curves were observed to be extremely dependent on the tip potential, as seen in Figure 3.

Below a tip potential value of 0 V/SCE, virtually no current other than tunneling was recorded. However, as the tip potential increased, so did the magnitude of the tip current approach curves until the tip potential reached ~0.3 V/SCE, where the current ceased to increase with the tip potential. The resulting S-shaped variation of i_{peak}, the peak height of the tip current approach curve, as a function of the tip potential is plotted in the inset of Figure 3. In the following, unless otherwise stated, tip current approach curves were recorded with a tip potential $E_{tip} > 0.3$ V/SCE, which is sufficiently high for the current approach curve not to depend on the exact value of E_{tip}.

Cyclic Voltammetry with the Tip inside the Few-Nanometers-Thick End-Grafted Fc-PEG Layer. The positioning capabilities of the AFM instrument were used to position the tip within the Fc-PEG layer at a predefined distance from the substrate surface. Using the programmable interface of the AFM controller, the following automated sequence was executed (see Experimental Section for details). The tip was pulled away from the substrate by a predefined amount, biased to an initial potential of -0.05 V/SCE, and a cyclic voltammogram was recorded at a relatively high scan rate of 0.5 V/s so that the thermal drift of the piezo during the voltamogram was minimized. At this stage, the tip-biasing circuit was opened. The tip was then brought back in contact with the substrate and retracted again. The resulting deflection approach curve was used to determine accurately d, the distance at which the voltammogram was recorded. As shown in Figure 4a, when the tip was positioned 30 nm away from the surface, a purely capacitive signal was recorded.

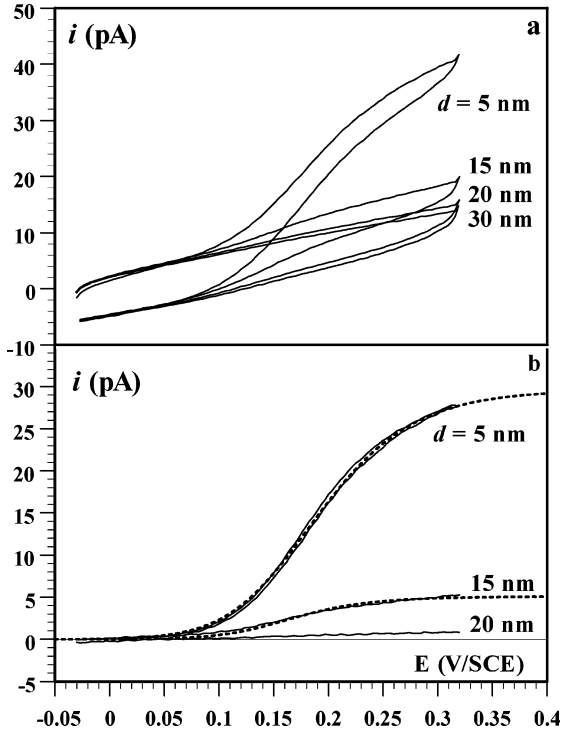

Figure 4. Cyclic voltammetry within the Fc-PEG macromolecular layer. The AFM-SECM tip is positioned at a tip-to-substrate distance d from the PEG-modified substrate, and the tip potential is scanned at 0.5 V/s. Unprocessed (a) and background-subtracted (b) voltammograms recorded at various d. The dotted lines correspond to theoretical voltammograms computed from eq 9 with $\Lambda = 0.57$ and 1.35 for $d = 5$ and 15 nm, respectively.

But when the tip was positioned closer to the surface, the voltammogram developed a typical sigmoid shape. This is made even more obvious in Figure 4b, where the voltammogram recorded at 30 nm is used as a background and subtracted from the voltammograms recorded with the tip positioned within the layer. The height of the plateau current of the S-shaped voltammogram was observed to depend strongly on d: the closer the tip-to-substrate distance, the more intense the plateau current. During these in situ cyclic voltammetry experiments, the substrate potential was kept constant at -0.1 V/SCE.

Effect of the Surface Coverage of Fc-PEG Chains on the Approach Curves. AFM-SECM experiments were conducted over gold surfaces bearing Fc-PEG chains at given surface concentrations ranging from 0.5×10^{-11} to 2×10^{-11} mol/cm^2. In every case, the deflection curves thus obtained resembled

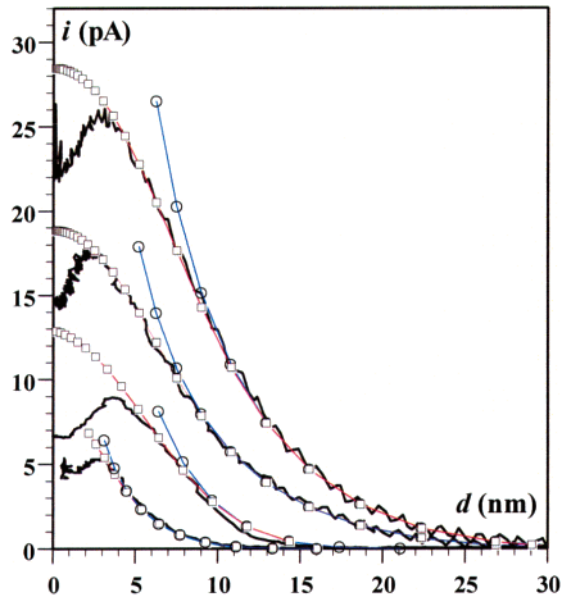

Figure 5. Current−distance approach curves at various Fc-PEG surface coverages Γ. The approach curves (thick lines) recorded for, from top to bottom, Γ (× 10^{11} mol/cm^2) = 2, 1.25, 0.9, are 0.5 are fitted using eq 7, which does not take chain compression into account (○), and using eq 8, which does take compression into account (□). The fitting parameters correspond to d^*, i^*, d_c, χ sequence values of 15 nm, 19 pA, 7.5 nm, 3; 14 nm, 10 pA, 6.7 nm, 3; 10 nm, 13 pA, 5 nm, 3; and 5.6 nm, 6 pA, 3.5 nm, 3 (top to bottom). E_{tip} = +0.4 V/SCE; E_{sub} = −0.1 V/SCE; 1 M $NaClO_4$ supporting electrolyte.

the one reported in Figure 2b, but could only be quantitatively exploited for the highest surface concentration explored, as detailed below. The current approach curves were observed to be strongly dependent on the Fc-PEG surface coverage. Not only did the current intensity increase with the surface concentration of Fc heads (Figure 5), but the current was observed to drop to zero much farther away from the surface at high rather than at low Fc-PEG surface concentration (compare the tip current approach curves in Figure 5 for Γ = 0.5 × 10^{-11} and 2 × 10^{-11} mol/cm^2).

Discussion

Structural Characterization of the PEG Layer. (a) Measurement of the Chain Surface Coverage. As explained above and detailed in the Supporting Information, the integration of the voltammetric signals recorded at the Fc-PEG derivatized substrate yields the total amount of chains present on the substrate and ultimately Γ the chain surface coverage, provided that the effective surface area of the substrate is known. The theoretical variation of the conformation of end-grafted linear flexible chains as a function of their surface coverage has initially been approached by scaling arguments.[1a,b] When the chains are grafted onto the surface sufficiently far apart that they do not interact, the average height, h, of the polymer layer is given by the Flory radius, R_f, of the chains in solution: $h = R_f = aN^{3/5}$, N being the degree of polymerization of the chain and a the monomer size. At higher coverage, when s, the average distance between the grafting point of the chains, approaches R_f, the chains start to interact and stretch toward the solution, forming a polymer brush. This occurs at a critical value of $s = R_f$, corresponding to a critical dimensionless coverage, $\sigma_{mushroom}$, given by $\sigma_{mushroom} = (a/R_f)^2 = N^{-6/5}$. When the coverage σ exceeds this limit, the brush height is given, to within an unknown prefactor of the order of unity, by[1a,b]

$$h \sim Na\sigma^{1/3} \quad (1)$$

In the present case, $N \approx 79$; thus, taking $a = 0.37$ nm,[20b,23] we have $\sigma_{mushroom} = 5.4 \times 10^{-3}$, and as by definition $\sigma = (a/s)^2 = (N\Gamma)a^2$, this translates into $\Gamma_{mushroom} = 0.7 \times 10^{-11}$ mol/cm^2.

In the present work, Γ ranges from 0.5 × 10^{-11} to 2 × 10^{-11} mol/cm^2, so we expect the conformation of the polymer layer to respectively range from a mushroom to a loose brush conformation.

Estimation of the Polymer Layer Height from the Force Approach Curve. The tip movement vs tip−substrate separation AFM deflection approach curves, such as the one reported in Figure 2b, can be converted into classical force (F) vs distance curves once the spring constant, k_{probe}, of the AFM-SECM combined probe is known, since $F = k_{probe}Z_{tip}$. The spring constant of each combined probe used in this study was determined geometrically as described in the Experimental Section, and force curves such as the one reported in Figure 6a were constructed.

The structure of end-grafted polymeric layers in good solvents has previously been studied by AFM-based techniques, and force curves similar to the ones obtained in the present work are reported in the literature.[24] The compression of the polymer layer in a good solvent can be quantitatively analyzed in terms of the following formula that relates the force applied to the layer, F, to the tip-to-substrate distance, d, by[22,24a,c,25]

$$F \approx \{100hR_{tip}k_bT/s^3\}\exp(-2\pi d/h) \quad (2)$$

with R_{tip} the tip radius, k_b the Boltzman constant, and T the temperature.

However, the above expression is expected to be valid only for the brush case and is also defined within an undefined factor of the order of unity. Indeed, the linear variation of ln(F) vs d predicted by eq 2 was observed only for the highest surface coverage we could explore, Γ = 2 × 10^{-11} mol/cm^2 (see inset of Figure 6a). Least-squares fitting of this ln(F) vs d variation then leads to h = 12.4 nm and s = 3.5 nm (taking R_{tip} = 225 nm as measured by scanning electron microscopy imaging of the tip, see Experimental Section). These numbers can be compared with the ones deduced from eq 1 (taking an implicit prefactor of unity) and from the value of Γ: $h \approx 7.3$ nm and $s \approx 2.8$ nm. It appears that the h value determined from the force curve analysis is larger than expected. This falls in line with literature reports that have consistently shown that the use of eq 2 leads to coherent albeit overestimated height for end-grafted polymer layers.[24a,c] In contrast, the values found for s seem quite reasonable and consistent one with another, especially if one takes into account that the ±50% error margin on the value of the spring constant of our homemade AFM probes contributes to a systematic error of ±20% on the value of s as determined from eq 2. Conversely, the experimental h value, being determined from the slope of the logarithmic variation of F with

(23) Kenworthy, A. K.; Hristova, K.; Needham, D.; McIntosh, T. J. *Biophys. J.* **1995**, *68*, 1921−1936.
(24) (a) O'Shea, S. J.; Welland, M. E.; Rayment, T. *Langmuir* **1993**, *9*, 1826−1835. (b) Ortiz, C.; Hadziioannou, G. *Macromolecules* **1999**, *32*, 780−787. (c) Garnier, L.; Gauthier-Manuel, B.; van der Vegte, E. W.; Snijders, J.; Hadziioannou, G. *J. Chem. Phys.* **2000**, *113*, 2497−2503.
(25) (a) de Gennes, P. G. *C. R. Acad. Sci. (Paris)* **1985**, *300*, 839−843. (b) de Gennes, P. G. *Adv. Colloid Interface Sci.* **1987**, *27*, 189−209.

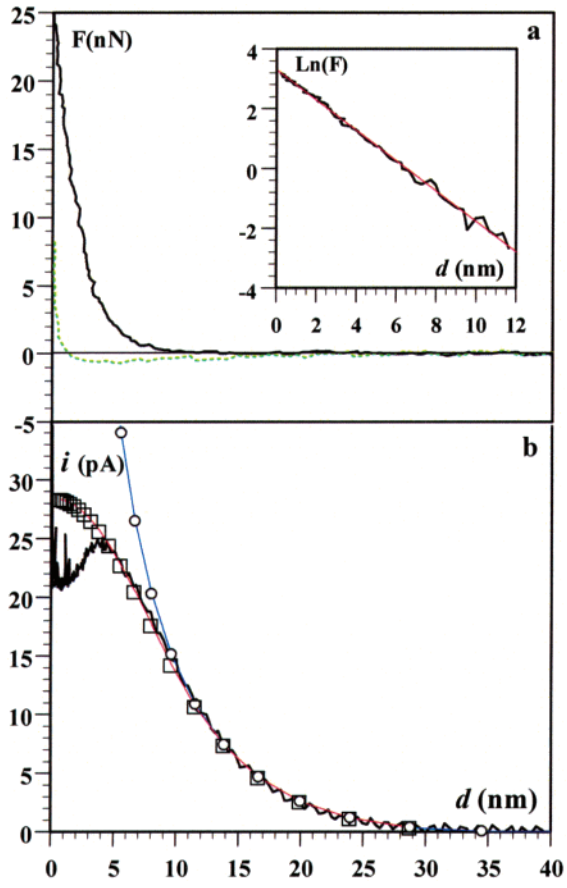

Figure 6. Simultaneously acquired force and current versus distance approach curves for a Fc-PEG layer. (a) Raw force curve; the corresponding linearized ln(*F*) vs *d* plot is shown in the inset. The dotted line represents the raw force curve recorded when the gold substrate bears only a cysteamine layer (no PEG chains present). (b) Experimental (thick continuous line) and theoretical (□, ○) current approach curves. The experimental current approach curve is fitted using the model of elastic bounded diffusion SECM positive feedback either neglecting (eq 7, ○) or explicitly taking into account (eq 8, □) the compression of the chains by the tip. The fitting parameters are $d^* = 15$ nm; $i^* = 19$ pA; $d_c = 7.5$ nm; $\chi = 3$. $\Gamma = 2 \times 10^{-11}$ mol/cm^2; $k_{probe} \approx 0.8$ nN/nm; $E_{tip} = +0.4$ V/SCE; $E_{sub} = -0.1$ V/SCE; 1 M $NaClO_4$ supporting electrolyte.

d, is not expected to be affected by the uncertainty on the value of the cantilever spring constant nor by the unknown prefactor value of eq 2.

At lower surface concentration of PEG chains, the above analysis of the force curve was not possible, as ln(*F*) vs *d* plots were observed to be no longer linear.

Quantitative Characterization of the SECM Electrochemical Approach Curves: Elastic Bounded Diffusion SECM Positive Feedback. (a) Characterization of the Faradaic Nature of the Tip Current. The nature of the tip current recorded when the tip was approached within 30 nm of a substrate bearing Fc-PEG chains can be identified as follows. The S-shaped potential dependence of the tip current approach curves presented in the inset of Figure 3 is typical of a Faradaic process[26] and is also extremely different from the exponential dependence expected for a tunneling process.[27] Moreover, the

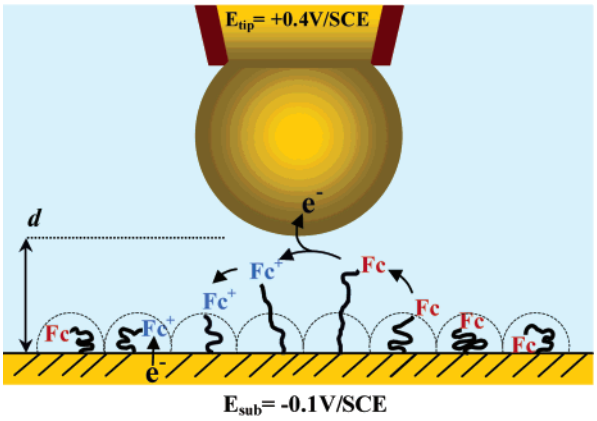

Figure 7. Schematics of the tip-to-substrate back-and-forth motion, and associated electron transfers, of the PEG-borne ferrocene (Fc) heads giving rise to the elastic bounded diffusion positive feedback current. For clarity, the tip is not drawn to scale. The chains are pictured in the mushroom conformation.

cyclic voltammograms recorded at the tip while its extremity was positioned in the polymer layer (see Figure 4) are typical of an electrochemical reaction taking place at a microelectrode,[28] and their characteristic half-wave potentials values ($E_{1/2}$) are close to the standard potential of the Fc/Fc^+ head (~150 mV/SCE). This allows us to attribute unambiguously the Faradaic process responsible for the tip current to the Fc head's electrochemistry. Finally, the current signal is observed only when the grafted PEG chain is end-labeled with an electroactive moiety such as Fc and when the tip is positioned at an altitude of less than ~30 nm above the substrate, i.e., a distance that corresponds nicely to the fully extended length, *L*, of the PEG_{3400} ($L = aN = 29$ nm). We therefore assign the current approach curves recorded here to the occurrence of a back-and-forth movement of the Fc heads between the tip and substrate, as schematized in Figure 7.

The ferrocene heads shuttle the electrons from the substrate to the tip, thus giving rise to the tip current in a SECM positive feedback process, usually observed for solution species.[8] When the tip and substrate potentials are respectively positive and negative enough with respect to the ferrocene head standard potential, the intensity of the feedback current is solely conditioned by the rate of the ferrocene head's cycling motion, which is kinetically controlled by the flexibility of the PEG chains. Quantitative analysis of the positive feedback response can thus give access to the dynamics of the PEG chains within the layer.

(b) The Elastic Bounded Diffusion Model. The AFM-SECM experiments reported here specifically address the motion of the Fc head perpendicular to the substrate, so we will restrict the formulation of the analysis of the dynamics of the system to this sole dimension. We make use of the elastic bounded diffusion model we previously introduced,[13,20] which describes the dynamics of the Fc head in terms of the friction of the chain on the solvent (via a diffusion coefficient *D*) and of the restoring force of the chain (via a chain spring constant k_{spr}). We start by calculating the stationary current, i_{TLC}, expected for a thin layer cell-like (TLC) configuration,[29] where the chains are sandwiched between the anchoring plane and a planar tip located at an altitude d_{TLC} above it (see Figure 8a).

(26) Bard, A. J.; Faulkner, L. R. *Electrochemical Methods. Fundamentals and Applications*; Wiley: New York, 1980.
(27) (a) Pan, J.; Jing, T. W.; Lindsay, S. M. *J. Phys. Chem.* **1994**, *98*, 4205−4208. (b) Vaught, A.; Jing, T. W.; Lindsay, S. M. *Chem. Phys. Lett.* **1995**, *236*, 306−310. (c) Halbritter, J.; Repphun, G.; Vinzelberg, S.; Staikov, G.; Lorenz, W. J. *Electrochim. Acta* **1995**, *40*, 1385−1394.
(28) Amatore, C. In *Physical Electrochemistry. Principles, Methods and Applications*; Rubinstein, I., Ed.; Marcel Dekker: New York, 1995; p131.208.

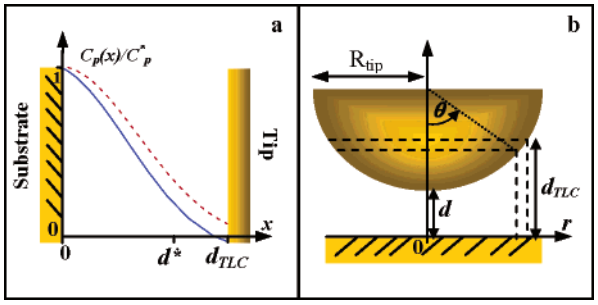

Figure 8. Calculation of the elastic bounded diffusion positive feedback. (a) Planar tip vs planar substrate TLC configuration. Concentration profiles of Fc heads as derived from the elastic bounded diffusion model, at equilibrium (dashed line, eq 4) and during feedback (continuous line, eq 6). x is a space variable varying from 0 to d_{TLC}. (b) Spherical tip vs planar substrate configuration. Integration over the lower half of the spherical tip of the feedback current due to each elementary concentric ring of radius r, acting as a planar TLC of height d_{TLC}, yields the elastic bounded positive feedback response for such a configuration.

According to the elastic bounded diffusion model, the modified second Fick's law, describing the time and space dependence of the volume concentration, C_P, of the ferrocene head (noted P) within the tip−substrate gap, is

$$\frac{\partial C_P}{\partial t} = D\left[\frac{\partial^2 C_P}{\partial x^2} + \frac{k_{spr}}{RT}\frac{\partial (xC_P)}{\partial x}\right]$$

where t is the time and x is the space variable measured from the surface and toward the solution.

The general expression of the flux, $J(x,t)$, of P heads going from the substrate to the tip is related to the concentration of P heads by

$$J(x,t) = -D\left[\frac{\partial C_P}{\partial x} + \frac{k_{spr}}{RT}C_P x\right] \qquad (3)$$

Here we are only interested in the expression of the time-independent (i.e., stationary: $\partial C_P/\partial t = -\partial J/\partial x = 0$) values of J and $C_P(x)$, which can be obtained by integration of the differential eq 3 as follows.

When no current flows (i.e., no anodic potential applied to the tip), $J = 0$ and resolution of the first-order linear differential eq 3 yields

$$C_P(x) = C^*_P \exp\left[-\frac{k_{spr}}{2RT}x^2\right] \qquad (4)$$

with $C^*_P = C_P(x = 0)$ as the integration constant.

C^*_P, the concentration profile of P heads at the substrate surface, can be found by integration of $C_P(x)$ for every x value ranging from $x = 0$ up to $x = d_{TLC}$, which yields the surface concentration of Fc heads, Γ: $\int_{x=0}^{d_{TLC}} C_P(x)\, dx = \Gamma$.

From this it ensues that

$$C^*_P = \Gamma\sqrt{2k_{spr}/\pi RT}/\mathrm{erf}(d_{TLC}\sqrt{k_{spr}/2RT})$$

Therefore, the ferrocene head concentration profile at equilibrium is predicted to be given by a Gaussian curve centered on the substrate surface (see dashed curve in Figure 8a). This Gaussian profile results from the extremely simplified description of the chain dynamics by the elastic bounded diffusion model. This model can be improved to accommodate for the offset of the maximum of the ferrocene head concentration profile away from the anchoring surface, which is predicted by theory and simulations,[2d−g,6a,b] as detailed in the Supporting Information. It is shown that, considering the relatively low coverage values explored here, this has little impact on the elastic bounded feedback current, as calculated below.

When potentials applied to the tip and the substrate are respectively positive and negative enough compared to the standard potential of the Fc/Fc^+ redox couple, a current will flow through the system (J = constant).

At the tip ($x = d_{TLC}$), the Fc (P) heads are oxidized to their Fc^+ counterpart (noted Q), that is,

$$P \rightarrow Q + e^-$$

and thus $C_P(x = d_{TLC}) = 0$.

Whatever x, Q and P heads' concentrations are related by a conservation equation:

$$C_P(x) + C_Q(x) = C^0_P(x)$$

At the substrate ($x = 0$), Q heads are reduced back to their P form:

$$Q + e^- \rightarrow P$$

and thus $C_Q(x = 0) = 0$; hence, $C_P(x = 0) = C^*_P$.

Using these boundary conditions, integration of the differential eq 3 then yields the following expression for the stationary flux of P heads:

$$J = \frac{DC^*_P}{\int_0^{d_{TLC}} \exp\left[\frac{k_{spr}}{2RT}x^2\right] \partial x}$$

so that finally

$$J = \frac{D\Gamma k_{spr}/\sqrt{\pi RT}}{\mathrm{erf}(\gamma)\ \mathrm{erfi}(\gamma)}$$

with the erfi function being defined as

$$\mathrm{erfi}(x) = \int_0^x e^{y^2} dy; \quad \gamma = d_{TLC}\sqrt{k_{spr}/2RT}$$

γ is a dimensionless parameter that compares the tip-to-substrate distance, d_{TLC}, to d^*, a chain spring constant-related characteristic layer thickness, given by

$$d^* = \sqrt{2RT/k_{spr}}$$

As can be seen from eq 4, d^* characterizes the width of the equilibrium Gaussian chain head distribution away from the surface. The resulting Faradaic feedback current is then simply given by

$$i_{TLC} = FSJ = \frac{FSD\Gamma k_{spr}/\sqrt{\pi RT}}{\mathrm{erf}(\gamma)\ \mathrm{erfi}(\gamma)} \qquad (5)$$

with S the tip surface.

(29) Hubbard, A. T.; Anson, F. C. In *Electroanalytical Chemistry*; Bard, A. J., Ed.; Marcel Dekker: New York, 1982; Vol. 4, pp 130−131.

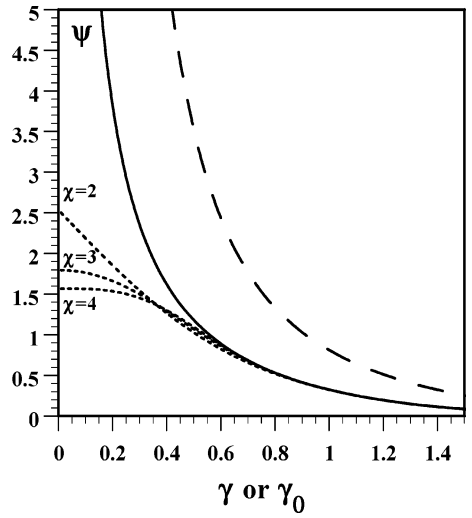

Figure 9. Universal elastic bounded diffusion SECM positive feedback approach curves. The dimensionless tip current ψ is plotted as a function of the dimensionless tip−substrate distance γ (or γ_0, see text). The chains are end-tethered to a planar substrate, and the motion of their free redox heads is described in the framework of the elastic bounded diffusion model. The dashed line is the calculated feedback curve for a planar tip, and the continuous line is for a spherical tip (the tip radius is assumed to be very large when compared to the chain length). The theoretical dotted lines consider a spherical tip situation with a distance dependence of the diffusion coefficient for the loose ends and are computed for different values of χ with $d_c = 0.5d^*$.

Proceeding as described above, integration of eq 3 from the substrate surface to any position x within the tip−substrate gap leads to the following expression for $C_P(x)$, the ferrocene head concentration profile during feedback, which is plotted in Figure 8a and given by

$$C_P(x)/C_P^* = \exp\left(-\frac{k_{spr}}{2RT}x^2\right)\left[1 - \mathrm{erfi}\left(x\sqrt{\frac{k_{spr}}{2RT}}\right)/\mathrm{erfi}\left(d_{TLC}\sqrt{\frac{k_{spr}}{2RT}}\right)\right] \quad (6)$$

The dimensionless elastic bounded positive feedback current approach curve predicted for a planar tip approaching a planar substrate can be represented by a plot giving ψ, defined as

$$\psi = i_{TLC}\sqrt{\pi}RT/FSD\Gamma k_{spr} = 1/\mathrm{erf}(\gamma)\,\mathrm{erfi}(\gamma)$$

as a function of γ and is shown in Figure 9 (dashed curve). As can be seen a sharp, distance dependence of the current is predicted as when $\gamma \to 0$, $\psi \to +\infty$, whereas when $\gamma > 1$, ψ decreases rapidly to zero.

As explained in the Experimental Section, the tips used here are extremely smooth submicrometer-sized spherical microelectrodes. To accommodate for such a tip geometry, we integrated the above expression over the lower half surface of a spherical tip. The substrate beneath the tip is divided in elementary concentric rings of radius r and of surface ∂S, centered around the tip axis. Each ring is assumed to form an elementary thin-layer cell, with the stripe of the tip located directly above it at a distance d_{TLC} (see Figure 8b), and therefore contributes to the current by an amount ∂i given by eq 5:[30]

$$\partial i = \frac{FD\Gamma k_{spr}/\sqrt{\pi}RT}{\mathrm{erf}(\gamma)\,\mathrm{erfi}(\gamma)}\partial S$$

with

$$\partial S = 2\pi r\,\mathrm{d}r = 2\pi R_{tip}[1 - (d_{TLC} - d)/R_{tip}]\,\partial d_{TLC}$$

as

$$r = \sqrt{R_{tip}(d_{TLC} - d)[2 - (d_{TLC} - d)/R_{tip}]}$$

After integration over the tip surface, taking into account that the tip radius is much larger than the feedback distances (i.e., $(d_{TLC} - d)/R_{tip} \ll 1$), we derive the following expression for the elastic bounded feedback current at a spherical tip:

$$i = i^*\int_{\gamma_0}^{\gamma_{max}} \frac{\partial\gamma}{\mathrm{erf}(\gamma)\,\mathrm{erfi}(\gamma)} \quad (7)$$

with

$$i^* = 2\pi FDR_{tip}\Gamma\sqrt{2k_{spr}/\pi RT}$$

a characteristic current, and

$$\gamma_0 = d\sqrt{k_{spr}/2RT} = d/d^*$$

a dimensionless tip−substrate distance comparing d, the tip−substrate separation as defined so far, to d^*. γ_{max} is the dimensionless maximum elongation of the chains; it depends on L, the length of the fully stretched chains, as

$$\gamma_{max} = L\sqrt{k_{spr}/2RT} = L/d^*$$

We observed that the values calculated for the integral appearing in eq 7 did not depend on the exact value of γ_{max}, provided that $\gamma_{max} \geq 1.5$, a condition always fulfilled here. This is obviously due to the very fast decay of the ferrocene head concentration with distance, predicted by eq 4: only the ferrocene heads that can reach the tip surface within a distance $\gamma \leq 1.5$ significantly contribute to the current (see Figure 9). As a result, in what follows we take $\gamma_{max} = +\infty$.

Numerical evaluation of the integral appearing in eq 7 allows the universal elastic bounded feedback "spherical tip-toward-planar substrate" approach curve to be obtained by plotting $\psi = i/i^*$ as a function of γ_0 (see continuous curve in Figure 9). As expected, the approach curve thus predicted is not quite as steep as the one derived in the case of a planar tip. Nevertheless, a marked current increase is also expected when $\gamma_0 < 1$.

Determination of the Characteristic Distance, *d, and of the Diffusion Coefficient, *D*, of the Grafted Chains from the Elastic Bounded Diffusion Positive Feedback Response.** As can be seen in Figure 6b, for $d > \sim 10$ nm, a very satisfying adjustment can be obtained between the experimental current approach curve and the theoretical elastic bounded feedback current approach curve predicted by eq 7, provided that appropriate values are chosen for i^* and d^*. In other words, the theoretical curves given in Figure 9 are adjusted onto the experimental approach curves simply by converting the γ_0 and ψ axes into their d and i counterparts as $i = i^*\Psi$ and $d = \gamma_0 d^*$. Although this is actually a two-parameter fitting, the set of i^*,d^* allowing a good fit of the data was found to be unique once we

(30) A similar calculation method has been successfully used to assess the effect of tip shape on SECM feedback response of solution species, see: (a) Davis, J.; Fan, F.-R. F.; Bard, A. J. *J. Electroanal. Chem.* **1987**, *238*, 9−31. (b) Mirkin, M. V.; Fan, F.-R. F.; Bard, A. J. *J. Electroanal. Chem.* **1992**, *328*, 47−62.

limited ourselves to the adjustments for which the theoretical curve did not cross the experimental curve.[31] In the case presented in Figure 6, this leads to $d^* = 15 \pm 1$ nm and $i^* = 21 \pm 1$ pA. The value of D, the diffusion coefficient of the surface-grafted chains, can then be determined by calculating the product $i^*d^* = 4\sqrt{\pi}\, FDR_{tip}\Gamma$, using for R_{tip} the SEM-measured value of 225 nm. We thus obtain here a value of $D = (1 \pm 0.2) \times 10^{-7}$ cm^2/s.

Considering the end-to-end movement of the chain imposed by the tip-to-substrate travel of the ferrocene head, it seems quite reasonable to compare this value to the one predicted by the Rouse model,[32] which assumes that the friction due to the motion of each monomer is additive: $D_{Rouse} = D_{monomer}/N$. Taking for $D_{monomer}$ the diffusion coefficient of the ferrocene molecule in aqueous solution (which is similar in size to a monomer),[20b,23] we have $D_{Rouse} = 7 \times 10^{-6}/79 = 0.9 \times 10^{-7}$ cm^2/s, a value satisfyingly close to the diffusion coefficient we report here.

However, for tip−substrate distances d smaller than 5−10 nm, the experimental curves were observed to consistently lie below the approach curves predicted by eq 7. This can be attributed to the fact that the model developed so far does not take into account the effect of compression on chain dynamics. Indeed, comparing parts a and b of Figure 6, we see that only when a force corresponding to the compression of the polymer layer starts to be sensed does eq 7 cease to fit the data. An improved model, incorporating the effect of compression on the chain dynamics, is presented below.

Elastic Bounded Diffusion SECM Positive Feedback of Chains under Compression. (a) Introduction of a Tip−Substrate Distance-Dependent Diffusion Coefficient. Upon compression of the end-grafted layer, the chain concentration within the narrowing tip-to-substrate gap understandably increases, resulting in a rise of the local viscosity.[32c] Moreover, Monte Carlo simulations have shown that, when grafted chains are compressed, their degree of entanglement increases.[33] Both effects combine to lead to a gradual loss of the chains' mobility with increasing compression. To the best of our knowledge, no workable expression exists to quantify this compression-induced slowing phenomenon. Within the framework of the elastic bounded model chain dynamics being reflected by a diffusion coefficient, a slowing chain dynamics is to be represented by a decreasing diffusion coefficient. In an attempt to assess quantitatively the effect of this confinement-induced chain mobility loss on the elastic bounded positive feedback response, we thus introduce a tip-to-substrate distance-dependent diffusion coefficient, given by the following empirical expression:

$$D(d) = D\{1 - \exp[-(d/d_c)^{\chi}]\}$$

where d_c is a characteristic distance and χ is an exponent that decides the rate of this decay.

The above expression is chosen so that, beyond a characteristic tip−substrate distance d_c, the slowing effect of compression disappears, the chains being then uncompressed. However, at short tip−substrate distance, such that $d \ll d_c$, the diffusion coefficient sharply decreases with d, and the above expression then simplifies to $D(d) = D \times (d/d_c)^{\chi}$.

The theoretical expression for the elastic feedback approach curve, taking into account the above distance-dependent diffusion coefficient, is then obtained from eq 7, modified as follows:

$$\psi = i/i^* = \int_{\gamma_0}^{+\infty} \frac{(1 - \exp[-(\gamma/\gamma_c)^{\chi}])\partial\gamma}{\mathrm{erf}(\gamma)\,\mathrm{erfi}(\gamma)} \qquad (8)$$

where $\gamma_c = d_c/d^*$. Theoretical approach curves, calculated using the above expression, for several values of χ and for $\gamma_c = 0.5$ are plotted in Figure 9 (dotted lines).

One can see that, for a tip−substrate separation γ_0 such that $\gamma_0 > \gamma_c$, the calculated approach curve matches the one corresponding to a d-independent diffusion coefficient whatever the χ value. However, for $\gamma_0 < \gamma_c$, the modeled current increases much more slowly with decreasing γ_0 than in the case of a constant diffusion coefficient. The current is even predicted to level off for values of $\chi > 2$.

(b) Fitting the Experimental Current Approach Curves Taking into Account the Layer Compression. The experimental tip current approach curves can be fitted by the theoretical expression given by eq 8 as follows. The values of d^* and i^* are first determined by fitting the curves for $d > 10$ nm, where chain compression is negligible, using the theoretical approach curve given by eq 7 as described above. As shown in Figure 9, the characteristic distance, d_c, at which the approach curves calculated for a distance-dependent diffusion coefficient depart from the d-independent diffusion coefficient approach curve does not depend on χ, so d_c can be determined without any assumption about the value of χ. In the case of Figure 6, we thus find a value of $d_c = 7.5$ nm.

Once d_c is known, the value of χ that gives the best adjustment with the experimental approach curve is then determined for distances $d < d_c$. Restricting ourselves to integer values of χ, we find that a value of $\chi = 3$ is required in order to reproduce the curvature of the experimental curve. As can be seen in Figure 6, the introduction of a distance-dependent diffusion coefficient significantly improves the fit of the experimental current approach curve, and a very good agreement between theoretical and experimental current approach curves is possible even for short tip−substrate distances at which a significant compression of the chains, as reflected by the tip deflection, clearly occurs. This agreement simply shows that a decrease of the chains' mobility, as reflected by an apparent distance-dependent diffusion coefficient, can quantitatively account for the leveling off of the experimental elastic bounded diffusion feedback curves.

However, the simple models presented here do not explain the occurrence of a peak in the current approach curve that was systematically observed in the $d = 3$−4 nm region, for which a phenomenom other than chain slowing probably has to be invoked. This phenomenon is reversible, as the same peak is also observed when the tip is retracted away from the surface (see Figure 2c). It may tentatively be explained by some compression-induced conformational transition of the polymer chains present within the narrowing tip−substrate gap. Experi-

(31) In other words, we took into account at this stage that, because of the layer compression, the experimental curve always lay below the theoretical one, especially at short tip−substrate distance.

(32) (a) Doi, M.; Edwards, S. F. *The Theory of Polymer Dynamics*; Oxford University Press: Oxford, 1986; pp 91−96. (b) Grossberg, A. Y.; Khokhlov, A. R. *Statistical Physics of Macromolecules*; American Institute of Physics, New York, 1994; pp 224−236. (c) Grossberg, A. Y.; Khokhlov, A. R. *Statistical Physics of Macromolecules*; American Institute of Physics: New York, 1994; pp 245−266.

(33) Edvinsson, T.; Elvingson, C.; Arteca, G. A. *Macromol. Theory Simul.* **2000**, *9*, 398−406.

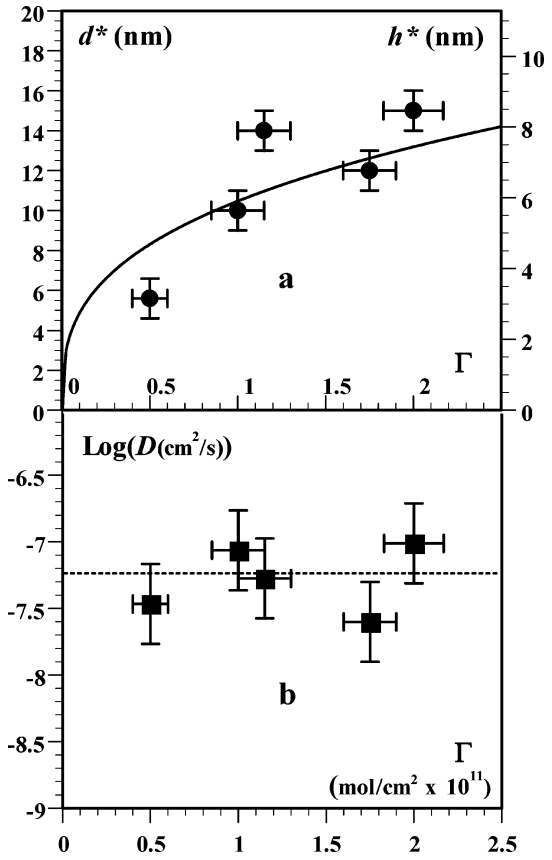

Figure 10. Chain surface coverage dependence of the characteristic parameters of the PEG_{3400} layer. (a) Measured characteristic distance d^* (left *Y*-axis) and average altitude of the ferrocene heads h^* (right *Y*-axis). (b) Evaluated diffusion coefficient of the loose ends of the grafted chains *D*. In (a) the continuous curve represents the theoretical variation $h \sim Na\sigma^{1/3} = Na^{5/3}(N\Gamma)^{1/3}$ as a function of Γ of the brush height, calculated for $a = 0.37$ nm, $N = 79$, and a numerical prefactor of 1. The horizontal error bars represent the uncertainty on each Γ value, determined as described in Supporting Information. The vertical bars in (a) represent the dispersion of the d^* value required to fit the 5−10 experimental tip current approach curves exploited for each experiment. The vertical bars in (b) represent the scatter of *D* values over all the experiments.

ments studying the compression of the Fc-PEG layers used here, using very sensitive commercial AFM probes, are currently being carried out to investigate this hypothesis.

Influence of the Chain Surface Coverage on the Structure and Dynamics of the Grafted Fc-PEG Layer. The dynamics and structural parameters of end-tethered Fc-PEG layers were determined from AFM-SECM experiments conducted at several chain coverages. In every case, a reasonable to very good fit between the experimental electrochemical approach curve and the theoretical elastic bounded positive feedback approach curve given by eq 7 is obtained for *d* values sufficiently large for the chain not to be notably compressed by the tip (see Figure 5). Series of d^* and *D* are thus obtained as described above for each chain coverage and plotted as a function of the corresponding surface concentration Γ in Figure 10.

As observed in Figure 10a, the experimentally determined d^* values increase slowly with the chain surface concentration. This reflects the thickening of the end-tethered layer with chain coverage as predicted by eq 1. However, as explained above, d^* characterizes the width of the Gaussian distribution of the ferrocene heads above the substrate surface and thus cannot be directly compared to the average layer thickness *h* given by eq 1. The appropriate parameter to compare to *h* is h^*, the average altitude of the ferrocene heads of the grafted chains, which can be calculated using the elastic bounded diffusion model as

$$h^* = 1/\Gamma \int_0^\infty x C_p(x)\, dx = d^*/\sqrt{\pi}$$

Once d^* values are converted into h^* values using the above expression, a reasonable agreement, represented as a continuous line in Figure 10a, is obtained between the experimental data and the *h* values calculated from eq 1 (using an implicit prefactor of 1). This result shows that, even though our model implies that the ferrocene heads are distributed throughout the grafted layer, their average position is close to the external edge of the layer.

The variation of the experimentally determined diffusion coefficient of the chains as a function of the chain coverage is presented in Figure 10b. It is seen that, within experimental uncertainty, no clear trend can be distinguished other than a roughly constant diffusion coefficient of $D = (6 \pm 4) \times 10^{-8}$ cm^2/s. This falls in line with the description of the end-to-end chain dynamics within the framework of the Rouse model, where the diffusion coefficient is not a function of coverage and is given by $D = D_{Rouse} \sim 1/(N\zeta^\circ)$, with ζ° the segment friction coefficient.[5b,6a] Even though it has been suggested that ζ° might depend on σ,[6b,d] it is expected to vary only slowly with the coverage as long as $\sigma < 0.05$.[6b] In either case, considering that the dimensionless coverage of the denser layer we studied was only of $\sigma = 0.016$, the constant value of *D* we report here is supported by theory and is, as predicted, close to the expected value of $D_{Rouse} = D_{monomer}/N = 9 \times 10^{-8}$ cm^2/s (see above).

At a tip-to-substrate distance close enough for the chains to experience compression by the tip, the introduction of a distance-dependent diffusion coefficient, as described above, allows us to account for the ensuing loss of chain flexibility, and eq 8 is then used to fit the approach curves recorded at several surface coverages. Keeping a constant value of $\chi = 3$, d_c is the only adjustable parameter, and eq 8 allows us to correctly fit the experimental curves for distances as small as $d \approx 5$ nm (see Figure 5). Values of d_c increasing from 3.5 to 7.5 nm were thus obtained for surface concentrations going from 0.5×10^{-11} up to 2×10^{-11} mol/cm^2.

This simply means that the slowing of the chains' motion is detected at a greater tip-to-substrate distance when the chain coverage is high rather than when it is low. Such a trend could have been expected as, for a given value of *d*, the tip−substrate gap gets understandably more crowded at high rather than at low surface coverage.

It is interesting to notice that, whatever the surface coverage, electrochemical approach curves remain peak-shaped, and additionally the position of the peak is roughly constant around a value of $d_{peak} = 3 \pm 1$ nm.

Finally, it is may also be enlightening to consider electron hopping between ferrocene heads as an alternative to the physical chain head motion to shuttle the electrons from the substrate to the tip. For a surface concentration $\Gamma = 2 \times 10^{-11}$ mol/cm^2, the local ferrocene head concentration within a $d \approx 3$ nm gap would be ~70 mM. This still corresponds to a very low fractional coverage of $\sim 5 \times 10^{-3}$, as defined in ref 34, for

(34) Blauch, D. N.; Savéant, J.-M. *J. Am. Chem. Soc.* **1992**, *114*, 3323−3332.

which physical diffusion is expected to largely dominate over electron hopping (see Supporting Information for details). Therefore, at higher tip−substrate separation, hopping is, a fortiori, not expected to contribute to charge transport. This illustrates that, as shown previously,[11,13,20a,c] charge propagation across distances that Fc-PEG chains can reach by simple elongation can be entirely attributed to the elastic bounded motion of the ferrocene heads. Electron hopping between neighboring Fc heads, which would imply long-range charge transport along the substrate surface, can also certainly be neglected as, considering the fast tip and substrate reactions as well as the short tip−substrate distance explored here, the diffusion field is necessarily orientated perpendicular to the substrate surface. Moreover, such a cylindrical surface diffusion-like process is predicted to give rise to transient currents[28] that were not detected here.

Cyclic Voltammetry within a ~5-nm Macromolecular Layer: Kinetic Parameter of the Electrode Reaction. Analysis of the background-subtracted positive feedback cyclic voltammograms recorded while the tip was positioned within the layer, a few nanometers above the substrate surface, can be performed as follows. The electrochemical reaction taking place at the tip, that is, the oxidation of the ferrocene heads, can be represented as

$$P \overset{E^\circ,\, k_s,\, \alpha}{\rightleftharpoons} Q + e^-$$

with α the Butler−Volmer transfer coefficient (taken here as α = 0.5) and k_s the heterogeneous rate constant for the electron transfer.[26]

The tip current, i, is related to the tip potential, E, by the following general theoretical expression, valid for any steady-state measurement:[35]

$$\frac{i}{i_{pl}} = \frac{1}{1 + \exp\left(-\frac{F}{RT}(E - E^\circ)\right) + \exp\left(-\alpha\frac{F}{RT}(E - E^\circ)\right)/\Lambda} \quad (9)$$

with i_{pl} the plateau current of the sigmoid-shaped voltammogram and Λ a dimensionless parameter comparing m, the transport rate of the heads, to the rate of electron transfer, $\Lambda = k_s/m$. In the present case, the ferrocene head motion being of a diffusional nature, it seems natural to take $m = D/d$, so that $\Lambda = k_s d/D$.[36]

The cyclic voltammograms recorded at tip-to-substrate distances of 5 and 15 nm can then be very satisfyingly fitted using the above expression (see dotted curve in Figure 4b). Taking an average value of $D = 6 \times 10^{-8}$ cm^2/s for $d = 15$ nm and a chain compression corrected value of $D = 4 \times 10^{-8}$ cm^2/s for $d = 5$ nm (see above) then yields a value of $k_s = (5 \pm 1) \times 10^{-2}$ cm/s. This value is in good agreement with the value of $(4 \pm 1) \times 10^{-2}$ cm/s measured by transient cyclic voltammetry for Fc-PEG coils in solution.[13]

Number and Distribution of the Chains Involved in the Elastic Bounded Feedback. A characteristic feature of the positive feedback is that the fast cycling of the redox species between the tip and substrate constitutes in itself an amplification mechanism that has been reported to even allow the detection of single molecules.[37] The number of ferrocene heads, that is, of PEG chains, involved in the elastic bounded feedback process observed here can be estimated by evaluating the current generated by the cycling of a single ferrocene head as follows. For a tip-to-substrate distance d, the tip-to-substrate diffusional transit time is $\tau = d^2/D$. One electron is exchanged at every cycle, so the current due to the motion of a single chain is given by $i = e/\tau = eD/d^2$ (e being the charge of an electron). Taking an average value of $D = 6 \times 10^{-8}$ cm^2/s, we find, for a typical distance d of 5 nm, $i \approx 0.04$ pA/chain. We thus conclude that some ~200 chains are required to generate the ~10 pA feedback currents we recorded. A more detailed calculation of the number of chains involved in the positive feedback process along with their radial distribution can be carried out, using the numerical evaluation of the integral appearing in eq 7, as follows.

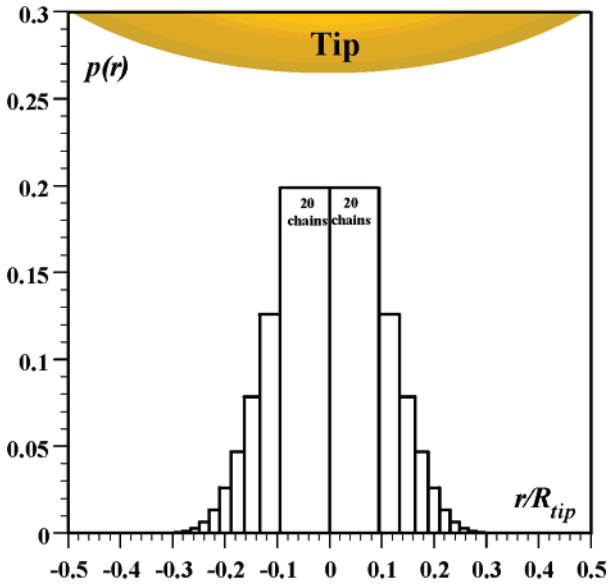

Figure 11. Elastic bounded diffusion positive feedback at a large spherical tip. Theoretical radial distribution of the chains contributing to the feedback current. The *Y*-axis represents the relative contribution to the total current of the ~20 chains represented by each bar. Calculated for $\Gamma = 0.5 \times 10^{-11}$ mol/cm^2, $R_{tip} = 225$ nm, and $d = d^* = 5.6$ nm.

The relative contribution to the overall current due to the chains located within the ring of width Δr, located at a radial distance r from the tip axis (see Figure 8b), is given by

$$p(r) = \int_{\gamma_1}^{\gamma_2} \frac{d\gamma}{\mathrm{erf}(\gamma)\,\mathrm{erfi}(\gamma)} \Big/ \int_{\gamma_0}^{+\infty} \frac{d\gamma}{\mathrm{erf}(\gamma)\,\mathrm{erfi}(\gamma)} \quad (10)$$

with $\gamma_1 = \gamma_0 + R_{tip}(1 - \cos(\theta))/d^*$, $\gamma_2 = \gamma_1 + \Delta\gamma$, $\Delta\gamma \approx 0.5\Delta r[2r + \Delta r]/R_{tip}d^*$ and $r/R_{tip} = \sin(\theta)$, θ being defined as shown in Figure 8.

The number of chains present within each ring can be approximated by $n_C = \pi\Delta r[2r + \Delta r]\Gamma = 2\pi R_{tip}d^*\Delta\gamma\Gamma$. The radial chain distribution thus calculated for $\Gamma = 0.5 \times 10^{-11}$ mol/cm^2, $R_{tip} = 225$ nm, and $d = d^* = 5.6$ nm is presented in Figure 11 as a bar graph, each bar amounting for the contribution of $n_c \approx 20$ chains.

As could be expected, the chains transporting the current are mostly localized below the very tip end of the spherical

(35) Mirkin, M. V.; Bard, A. J. *Anal. Chem.* **1992**, *64*, 2293−2302.
(36) In this approach, only the transport rate of the chains located under the very tip of the spherical microelectrode, which is separated by a distance d from the tip, is considered. This is valid as this transport rate is the fastest of all chains contributing to the current and thus decides the voltammogram quasi-reversible character through the value of Λ.
(37) (a) Fan, F.-R. F.; Bard, A. J. *Science* **1995**, *267*, 871−874. (b) Fan, F.-R. F.; Bard, A. J. *Acc. Chem. Res.* **1996**, *29*, 572−578. (c) Fan, F.-R. F.; Juhyoun Kwak, J.; Bard, A. J. *J. Am. Chem. Soc.* **1996**, *118*, 9669−9675.

microelectrode. Cumulating the contribution of the chains of each ring, we find that 90% of the current is due to ~160 chains localized within a distance of the tip axis of $r = 0.2R_{tip}$, which is in the present case 50 nm. This demonstrates the focusing effect of the elastic bounded feedback: the lateral resolution is only a fraction of the tip size and is governed by the chain elasticity. Similarly, but along the tip axis, one can calculate using eq 10 that the above 160 chains are sensing only the extremity of the tip, when positioned some ~5 nm above the substrate, over a height of ~6 nm.

Conclusion

We showed here that AFM-SECM allows us to quantitatively probe both the dynamics and the structure of end-tethered, redox-labeled linear polymer chains. When a microelectrode tip is approached from the flat anchoring substrate to within a distance of ~10−30 nm, the ferrocene heads are oxidized at the tip. The concentration gradient thus created drives the oxidized heads back to the substrate surface, where they are reduced. The ferrocene heads continuously shuttle electrons from the substrate to the tip; as a result, their cycling motion gives rise to measurable currents even when a very small number of chains is involved. To the best of our knowledge, no such positive feedback process of terminally anchored polymer chains has previously been reported. Using a model of elastic bounded diffusion that we had introduced previously and adapted here, the tip current response can be quantitatively analyzed, and both the layer thickness and the chain-head diffusion coefficient can be accessed. The thus-measured static and dynamic parameters are shown to vary with the chain surface coverage, Γ, as theoretically expected: the layer thickness increases as $\Gamma^{1/3}$, while the diffusion coefficient remains constant and close to the one predicted by the Rouse model. At short tip−substrate separation, a significant compression of the chains is detected by the force-sensitive combined probe, and the current then tends to level off. Such a behavior is due to the overcrowding of the tip-to-substrate gap by the chains and was modeled in a phenomenological way by introducing a compression-dependent diffusion coefficient. Theoretical investigations (simulations) and AFM experiments are still required to understand fully not only this phenomenon but also the systematic occurrence of a peak in the SECM approach curve for tip−substrate distances smaller than a fraction of the chain Flory radius.

Acknowledgment. The authors are thankful to Michel Druet for improvement of the AFM-controlled low-current bipotentiostat. Prof. Christian Bourdillon, from the Université de Technologie de Compiègne (Compiègne, France), is thanked for his help with the vapor deposition of gold onto mica.

Supporting Information Available: SEM characterization of a AFM-SECM probe; details on the substrate voltammetry and surface Fc-PEG coverage determination; effect of offsetting the chain head concentration profile on the calculated elastic bounded diffusion SECM feedback curve; evaluation of the electron hopping contribution to the tip−substrate charge transport. This material is available free of charge via the Internet at http://pubs.acs.org.

JA0493502